Delft University of Technology

Stationary Energy Storage Solutions and Power Management for Bus Fleet Electrification in Congested Grid Areas

Paternost, Rudolf F.P.; Diab, Ibrahim; Mouli, Gautham Ram Chandra; Ricco, Mattia; Bauer, Pavol; Grandi, Gabriele

Important note
To cite this publication, please use the final published version (if applicable).
Please check the document version above.

RESEARCH ARTICLE

Stationary Energy Storage Solutions and Power Management for Bus Fleet Electrification in Congested Grid Areas

RUDOLF F. P. PATERNOST[1], **IBRAHIM DIAB**[2], **(Member, IEEE),**
GAUTHAM RAM CHANDRA MOULI[2], **(Member, IEEE),**
MATTIA RICCO[1], **(Senior Member, IEEE), PAVOL BAUER**[2], **(Senior Member, IEEE),**
AND GABRIELE GRANDI[1], **(Senior Member, IEEE)**

[1]Department of Electrical, Electronic, and Information Engineering, University of Bologna, 40136 Bologna, Italy
[2]Electrical Sustainable Energy Department, Delft University of Technology, 2628 CD Delft, The Netherlands

Corresponding author: Mattia Ricco (mattia.ricco@unibo.it)

ABSTRACT In the presence of a catenary infrastructure, the transition from fossil fuel-based bus fleets to electric-powered ones can be facilitated through conventional trolleybuses or In-Motion-Charging trolleybuses, offering environmentally friendly and cost-effective solutions. However, grid congestion at traction substations (TSs) can limit this transition as the grid operator is incapable or unwilling to provide more capacity. As grid connection contracts are typically tallied and billed in periods of 15 minutes, stationary energy storage devices can prove useful in short-term buffering of the power demand. Consequently, more electrification projects can be rolled out under the same, or minimally extended grid contract. In this aim, this paper looks at validating energy storage as a means of enabling bus fleet electrification. It presents a power management strategy that controls the power exchange between the energy storage system (ESS) within the TS, specifically to manage the 15-minute average power. This strategy also serves as a tool for sizing the ESS with the minimum capacity required for the application. A case study for the city of Bologna, Italy, has been considered to validate the proposed approach. The findings indicate that billing contract power can be reduced by up to 41.7% when a storage device actuates in high-energy-demand substations. Furthermore, different types of Lithium-ion cells, including their second-life versions, are compared to determine the most beneficial options under limited cost and volume constraints. Recommendations are drawn on the exact scenarios where each type of cell is most beneficial.

INDEX TERMS Transportation, trolleygrids, in-motion-charging, energy storage, second-life batteries.

I. INTRODUCTION

Electrical grids are increasingly more congested with the rolling out of sustainable, electrified technologies such as electric vehicles and heat pumps [1], [2]. This congestion threatens energy transition, limiting the potential installation of more electrical loads and hindering the feasibility of electrifying loads such as diesel buses into electric buses. However, in many cases, the congestion is momentary and can be solved by properly sized and controlled energy storage systems (ESS). This solution has a particularly

interesting potential in transport grids which are typically oversized and underutilized, whereby the momentary congestion does not necessitate infrastructure updates. Indeed, many works are already rethinking trolleygrids as multi-functional, active grids by integrating renewable energy sources [3], [4], electric vehicle chargers [5], [6], smart loads and fleets [7], [8], [9], [10].

A. FLEET ELECTRIFICATION WITH IN-MOTION-CHARGING TROLLEYBUSES

A new generation of trolleybuses, namely the In-Motion-Charging bus (IMC) is seen as the future fleet of trolleygrids [10], [11], [12], [13]. IMC buses combine the
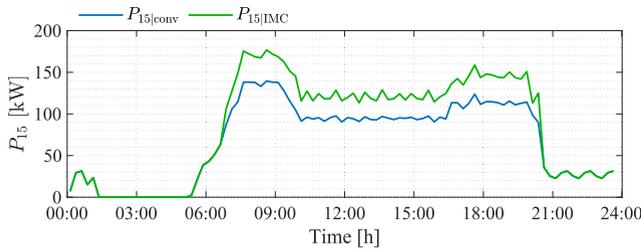
FIGURE 1. Values of the 15-minute average power, P_{15}, supplied by a TS for a one-day simulation of trolleybus operation in the case study of Bologna defined in this paper.

advantages of a conventional trolleybus and those of a battery electric bus (BEB) [14]. They operate under the catenary in a trolley-mode fashion but are also equipped with a relatively large on-board battery that is charged while the bus is in motion under this route segment. This battery is typically much smaller than the one adopted in a BEB, but still allows the IMC to operate for many kilometers out of the catenary. This gives the IMC bus both the route and range flexibility of a BEB but with a smaller battery size, needed only to cover the catenary-less part of the bus route. If a trolleygrid infrastructure is already in place, IMC buses become remarkably cost-effective [12]. Therefore, this manuscript focuses on the electrification of bus fleets using IMC trolleybuses in cities where catenary infrastructures are already available. Implementing BEBs in these cities is more complex, requiring a comprehensive analysis of variables such as charger positioning, and type of charging system (overnight or opportunity). However, while IMC buses offer advantages in terms of flexibility and cost-effectiveness, they also require significantly more power from the catenary infrastructure. Depending on the charging power, this can be up to six times per km more on average than the conventional trolleybuses [2], [12]. This constitutes a major hurdle for electrification projects as some congested areas of the trolleygrid cannot handle the additional power of an IMC bus.

B. CONGESTED GRIDS AND PROPOSED SOLUTION

The increase in grid congestion retains or incapacitates distribution system operators from expanding existing contracts of traction substations (TSs). However, the contractual power limit is typically based on the 15-minute average power demand (P_{15}) at the grid connection to the TS. This means that projects of bus electrification as IMC trolleybuses can still be feasible because some degree of freedom is afforded in the instantaneous power, as long as the P_{15} contractual limit is respected. For illustration, Fig. 1 shows the P_{15} increase due to IMC trolleybuses operation ($P_{15|IMC}$) in comparison to a case where only conventional ones operate ($P_{15|conv}$). The $P_{15|IMC}$ can be reduced by levels of $P_{15|conv}$ by a storage device that charges in moments of low loading on the TSs, and discharges in moments of high loading. Consequently, the new contract remains as close as possible to the existing one and to the capacity of the network operator. Otherwise, the required additional grid capacity could be untenable.

C. LITERATURE REVIEW AND RESEARCH GAPS

Many works exist on the topic of energy storage in traction grids. They are predominantly occupied with the reduction of energy consumption via the recuperation of braking energy, such as in [15], [16], [17], and [18], reduction of voltage drops [19], [20], [21], or peak shaving [22], [23], [24]. To achieve these goals, various energy storage solutions were explored. These works confine their analysis to one energy storage technology or compare different technologies with substantially different technical characteristics, like supercapacitors, batteries, and flywheels. Investigations conducted in [22] evaluated supercapacitors and Lithium-ion batteries for peak-shaving. In the same direction, manuscripts [23], [24] investigated supercapacitors, batteries, and flywheels. The aforementioned papers do not delve into details on intra-technology analyses within specific ESS categories.

Rather than shaving peaks for energy savings or reducing component ratings, this paper approaches a more practical and contemporary limitation to electrification: Grid congestion. This work presents a study concerned primarily with keeping the 15-minute power average, typical of grid contracts, under a certain limit. Furthermore, this paper compares multiple storage technologies for this aim. Specifically, the comparison takes into account ESSs built from Lithium-ion cells with Lithium Titanium Oxide as the anode (referred to as LTO), and Lithium-ion cells with Graphite as the anode and Lithium Iron Phosphate as the cathode (referred to as LFP). Both first and second-life systems are compared.

Indeed, both LTO and LFP belong to the lithium-ion battery family, however, they exhibit distinctions in terms of their performance characteristics. Both types are used in the automotive industry as the battery technology choice to power IMC trolleybuses. This research also conducts a comparative study between ESSs composed of new battery cells and ESSs composed of second-life batteries (SLBs) made by rearranging the decommissioned battery packs of IMC vehicles, to create an environmentally and economically virtuous circle.

D. PAPER CONTRIBUTIONS

To summarize, this paper offers:

1) The development of a tailored power-management scheme to reduce the P_{15} value to a user-defined level while simultaneously minimizing the required ESS size. This approach focuses on reducing the necessary volume and, indirectly, the cost of the storage device.

2) The comparative analysis of battery technologies, including their second-life (SL) versions, considering their differences in charge and discharge rates and internal resistances. The research encompasses comprehensive scenarios of TS power demand.

3) The derivation of a scheme aimed at aligning the performance of SLBs with that of new ones. This technique facilitates a fair comparison between them.
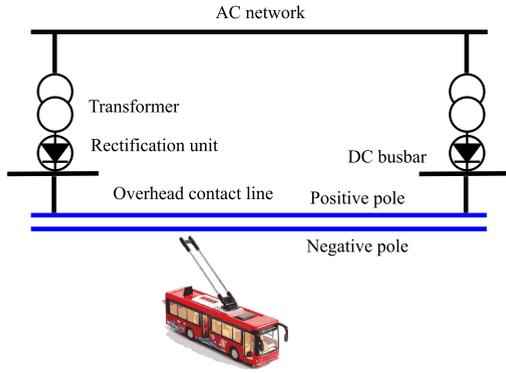
FIGURE 2. Electric schematic for powering DC catenaries.

E. PAPER STRUCTURE

The rest of this manuscript is arranged as follows. In Section II, the trolleybus system simulation procedure is presented, crucial for computing the power of TSs during a daily trolleygrid operation. Section III defines the objective of utilizing ESSs in TSs for the application proposed in this study and describes a control technique designed to regulate P_{15} to a user-defined value while simultaneously minimizing the ESS size. It also introduces the battery types under investigation and provides explanations on the consideration of SLBs in the analysis. Section IV presents the trolleybus system in Bologna, Italy, taken as the study case of this work, where IMC trolleybuses are expected to be in operation in the coming months. Section V presents the results of this work, where the analysis is conducted based on three situations defined based on the energy-intensive actuation of the storage device. Finally, conclusions are presented in Section VI.

II. TROLLEYBUS SYSTEM SIMULATION PROCEDURE

This section outlines the procedure for simulating a trolley-grid operation over time, which is essential to compute the power demanded by the trolleygrid in its TSs. This power is essential for a posterior calculation of the power managed by an ESS operating at a TS to regulate P_{15} to the desired level.

The trolleybus power flow simulation needs to consider three primary components, namely:

- The overhead contact lines (OCLs), comprised of both positive and negative conductors and the parallel (equipotential) lines connecting them.
- The electrical power supply infrastructure, consisting of the TSs and the connectors for linking to the OCLs.
- The loads, which refers to the moving vehicles connected to the OCLs via pantographs.

The DC power-flow analysis is based on categorizing the network nodes as power nodes or voltage nodes. Power nodes consider the power demand as the input, and voltage needs to be computed. Voltage nodes are defined the other way around. Trolleybuses are treated as power nodes, and their voltage is calculated via an iterative process. On the other hand, TSs are considered voltage nodes, and their voltage values
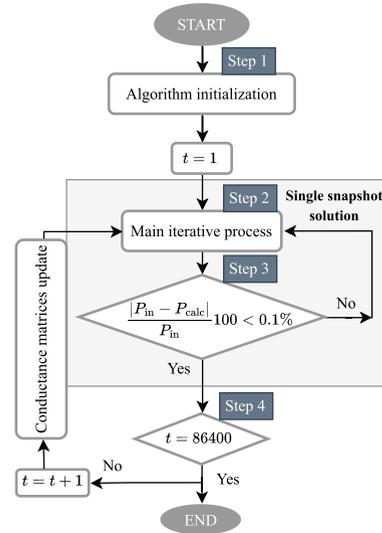
FIGURE 3. Flowchart of the trolleybus system simulation procedure.

are determined based on the nominal open-circuit voltage at the rectifier output (DC busbar), as depicted in Fig. 2. The voltage and current states of the DC network are linked by nodal conductance matrices, denoted as G, which are constructed for both the positive and negative poles. These matrices encompass information about the OCL resistance between nodes, network structure, and the positions of vehicles operating in the network, which change over time. The current injection or absorption at a specific node k can be represented as per [7], [25]:

$$I_k = V_k G_{kk} + \sum_{m \in \Omega_k} V_m G_{km}, \qquad (1)$$

where V_k is the voltage of node k, Ω_k is the collection of nodes m adjacent to node k having voltage V_m, with k that ranges from 1 up to the total count of nodes, denoted as N. Each component of the conductance matrix is given as:

$$G_{km} = G_{mk} = -\frac{1}{r_{km}}, \qquad G_{kk} = \sum_{m \in \Omega_k} \frac{1}{r_{km}}. \qquad (2)$$

The branch resistance between nodes k and m is denoted as r_{km}. Typically, a conductance matrix is sparse because $G_{km} = 0$ whenever there is no connection between the two nodes. The power injection or absorption at a given node k can be represented by the following equation:

$$P_k = V_k^2 G_{kk} + V_k \sum_{m \in \Omega_k} V_m G_{km}. \qquad (3)$$

The non-linear system in (3) is solved through a numerical method (e.g., Newton-Raphson). The simulation process is in steps of 1 second and summarized in the flowchart of in Fig. 3. The process is as follows:

Step 1: The algorithm initializes importing data about positions and power consumption of the trolleybuses. It also creates conductance matrices for both positive and negative
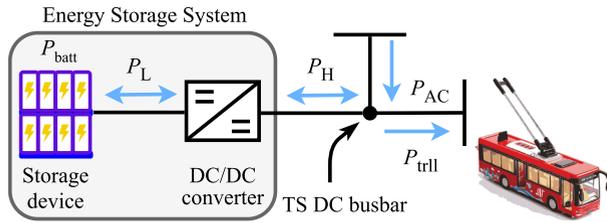
FIGURE 4. Schematic of the ESS connected to the DC busbar of a TS.

poles of the system. Additionally, a time counting the time of the day is initialized. The power values for the trolleybuses (P_{in}) are generated using a Simulink model that mimics the behavior of both conventional and IMC trolleybuses. Furthermore, the positions of the trolleybuses are determined based on the timetables of transportation companies.

Step 2: The main iterative process solves the non-linear system of equations (3), calculating the network voltages for the positive and negative poles. The trolleybuses' voltages are calculated based on the difference between their respective potentials at the positive and negative poles.

Step 3: The convergence is achieved when the percentage difference between the trolleybuses' input power (P_{in}) and the power values calculated (P_{calc}) through the iterative process falls below 0.1%.

Step 4: A check on the time counter (represented by t in Fig. 3) is performed to determine if the end of the day has been reached at which point the simulation stops. If not reached, the time counter and conductance matrices are updated to account for changes in the number, position, and power of the vehicles in operation.

III. ENERGY STORAGE SYSTEMS FOR ELECTRIFICATION PROJECTS IN CONGESTED GRID AREAS
A. PROBLEM FORMULATION
The objective of placing the ESS in a TS busbar (Fig. 4) is to control the 15-minute average power, P_{15}, ensuring it remains below a maximum value specified by the transportation company, named as reference power (P_{ref}). Hence, the power requested by the trolleygrid (P_{trll}) is less dependent on the power supplied by the AC network provider (P_{AC}). Consequently, is possible to minimize the increase between the maximum value of the 15-minute average power ($P_{15}^{\max}$) for the situation where bus fleets are electrified with IMC buses ($P_{15|\text{IMC}}^{\max}$), and its maximum value for the current situation, where only conventional trolleybuses operate ($P_{15|\text{conv}}^{\max}$).

The problem can be mathematically formulated as the minimization problem presented in (4), subject to the constraints defined in (5):

$$\text{Minimize: } (P_{15|\text{IMC}}^{\max} - P_{15|\text{conv}}^{\max}), \tag{4}$$

$$\text{Subject to: } \begin{cases} V_{\text{vol}|\text{ESS}} \leq V_{\text{vol}|\text{TS}} \\ \overline{C}_{\text{ESS}} \leq \overline{C}_{\text{TS}}. \end{cases} \tag{5}$$

$V_{\text{vol}|\text{ESS}}$ and $\overline{C}_{\text{ESS}}$ are the volume and cost of the ESS. $V_{\text{vol}|\text{TS}}$ is the volume available for the storage at the TS, and $\overline{C}_{\text{TS}}$ is the investment cost allocated by the transportation company for reinforcing the congested grid. To find the minimum solution for cost and volume, it is crucial to primarily understand the minimum ESS energy capacity required for the application. The scope of this work is limited to this initial evaluation, as presented in Section V.

The challenge in achieving the mentioned goal is to perform a proper charge and discharge scheme (C&D) of the ESS, since during discharge, P_{AC} is reduced, but during charge, it increases, as can be visually verified in Fig. 4:

$$\text{Charge} \rightarrow P_{\text{AC}} = P_{\text{trll}} + P_{\text{H}}, \tag{6}$$

$$\text{Discharge} \rightarrow P_{\text{AC}} = P_{\text{trll}} - P_{\text{H}}. \tag{7}$$

One way to control the power exchange between the ESS and the DC busbar is to charge the device during the night period when power demand is low and discharge at times of high demand. However, this leads to an oversizing of the device, violating volume and cost requirements. Therefore, this work considers that the charging process can happen at any time of the day and proposes a C&D scheme suitable for the desired application.

B. ENERGY STORAGE SYSTEM CHARGE AND DISCHARGE SCHEME
The power flow between the battery and the TS busbar is considered to be handled by a DC/DC converter. Therefore, the power balance of the battery during C&D can be described by the following relations:

$$\text{charge} \rightarrow P_{\text{batt}} = \eta_{\text{batt}} \cdot P_{\text{L}}, \tag{8}$$

$$\text{discharge} \rightarrow P_{\text{batt}} = \frac{1}{\eta_{\text{batt}}} P_{\text{L}}, \tag{9}$$

where P_{batt} is the power absorbed or injected by the battery during the charge and discharge process, respectively; P_{L} is the power flow between the battery and the low voltage side of the converter (Fig. 4), η_{batt} is the battery efficiency.

The power balance of the converter during C&D can be described by the following relationships:

$$\text{charge} \rightarrow P_{\text{L}} = \eta_{\text{conv}} \cdot P_{\text{H}}, \tag{10}$$

$$\text{discharge} \rightarrow P_{\text{L}} = \frac{1}{\eta_{\text{conv}}} P_{\text{H}}, \tag{11}$$

where P_{H} is the power flow between the converter's high voltage side and the substation busbar (Fig. 4); η_{conv} is the converter efficiency. P_{batt} and P_{H} can be put in relation by means of a round-trip efficiency (η_{rt}) of the compounded block composed by battery and converter:

$$\text{charge} \rightarrow P_{\text{batt}} = \eta_{\text{rt}} \cdot P_{\text{H}}, \tag{12}$$

$$\text{discharge} \rightarrow P_{\text{batt}} = \frac{1}{\eta_{\text{rt}}} P_{\text{H}}, \tag{13}$$

where the η_{rt} is defined as:

$$\eta_{\text{rt}} = \eta_{\text{batt}} \cdot \eta_{\text{conv}}. \tag{14}$$
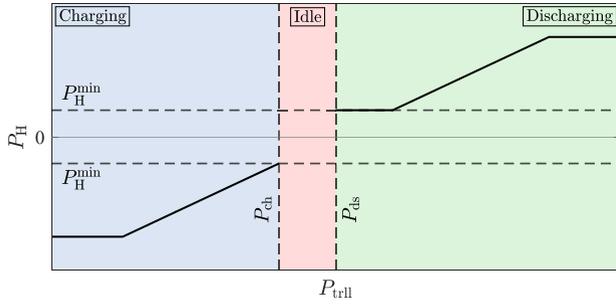
FIGURE 5. Control trans-characteristics for the ESS. Solid curves represent P_H; horizontal dashed lines indicate P_H^{min}; vertical dashed lines represent the idle region bounded by P_{ch} and P_{ds}.

For ensuring a high-efficiency operation of power electronics converters, the device should operate in a power range bounded by the converter's maximum (P_H^{max}) and minimum power (P_H^{min}), in which the efficiency value can be assumed between 94% and 96% [26]. This is because the efficiency of converters operating at low power levels tends to be lower compared to their efficiency at higher or full loads. For simplification purposes, in this study, η_{conv} is assumed to remain constant when operating within the range. That is:

$$\eta_{conv} = \text{constant} \qquad \text{if } P_H^{min} \leq P_H \leq P_H^{max}, \qquad (15)$$

where

$$P_H^{max} = P_{trll}^{max} - P_{ref}, \qquad (16)$$

$$P_H^{min} = \alpha \cdot P_H^{max}. \qquad (17)$$

P_{trll}^{max} is the maximum power requested by the trolleybus network in the situation without ESS operating in the TS; α is a percentage of the maximum power handled by the converter.

The ESS enters discharge mode when the power requested by the trolleybus network exceeds the upper threshold value, P_{ds}, defined here as numerically equal to P_{ref} (18). This happens in a high-loading scenario in the trolleybus network. On the contrary, when P_{trll} falls below the lower threshold value (P_{ch}), the ESS begins the charging process. The ESS remains idle, with zero power output, when P_{trll} is within the range between P_{ch} and P_{ds}. The idle region is defined in a way that ensures the converter's operation in its high-efficiency range. Therefore, P_{ch} and P_{ds} are defined as:

$$P_{ds} = P_{ref}, \qquad (18)$$

$$P_{ch} = P_{ds} - P_H^{min}. \qquad (19)$$

The ESS C&D modes are ruled by (20) and (21):

$$\text{charge} \rightarrow P_H = P_{ds} - P_{trll}, \qquad (20)$$

$$\text{discharge} \rightarrow P_H = \begin{cases} P_H^{min}, & \text{if } (P_{trll} - P_{ds}) < P_H^{min}, \\ P_{trll} - P_{ds}, & \text{if } (P_{trll} - P_{ds}) \geq P_H^{min}. \end{cases} \qquad (21)$$

Equation (20) shows that during the charging process, the power requested from the AC network will be equal to the

reference power ($P_{AC} = P_{ref}$), because of the definition of P_{ch} in (19). This ensures that the charging process happens already in maximum power conditions, minimizing the storage size required for the application. Equation (21) show that the ESS starts discharging from P_H^{min}, and follows the function in (21), only when P_H surpasses P_H^{min}. For illustration purposes, Fig. 5 depicts the charge and discharge characteristics. The power constraints imposed by the ESS C-rate result in a capped charge and discharge power.

C. SUGGESTED ENERGY STORAGE TECHNOLOGY SOLUTIONS

In general, LTO batteries can operate at high C&D rates. LFP batteries can also handle relatively high C&D levels, but cannot achieve the same level as LTO counterparts [27]. This work considers the continuous operation of LTO batteries up to 10C, and up to 5C for LFP ones. Despite the advantages in charge rates, LTO batteries possess a lower energy density when compared to LFP ones. Due to these different characteristics, it is important to verify whether batteries operating at high C&D rates have a significant advantage over those operating at lower levels. The C&D rates have particular importance because, for a given P_{ref}, a cell able to operate at larger C&D rates needs a smaller energy capacity to meet the power demand. Furthermore, the study assesses system performance utilizing second-life batteries (SLB).

Second-life batteries exhibit an increase in their internal resistance, leading to heightened energy losses during their C&D cycles. This phenomenon should result in a subsequent decrease in overall operational efficiency. Additionally, SLBs tend not to withstand C-rate operations at the same level as new batteries. Consequently, this manuscript explores the adjustment of the C-rate value in the operation of SLBs to neutralize the rise in internal resistance while assuring operational efficiency on par with brand-new batteries (NB).

Referring to Fig. 4, the loss (P_{loss}) incurred during discharge process is expressed as:

$$P_{loss} = P_{batt} - P_L = r_{batt} \cdot I_{batt}^2, \qquad (22)$$

where r_{batt} is the battery internal resistance; I_{batt} and P_{batt} are the current and power provided by the battery during discharge. Referring to (9), (22) can be written as:

$$P_{loss} = P_{batt} - \eta_{batt} \cdot P_{batt}. \qquad (23)$$

The battery efficiency is given as:

$$\eta_{batt} = 1 - \frac{P_{loss}}{P_{batt}} = 1 - \frac{r_{batt} \cdot I_{batt}^2}{V_{batt} \cdot I_{batt}}, \qquad (24)$$

where V_{batt} is the battery voltage.

The objective is to maintain the operational efficiency of SLBs on par with new ones. This involves counteracting the rise in internal resistance. The solution proposed is to reduce the current of SLBs (I_{batt}^{SL}) by a factor $\gamma < 1$ in relation to the current of NBs (I_{batt}^{NB}):

$$I_{batt}^{SL} = \gamma \cdot I_{batt}^{NB}. \qquad (25)$$
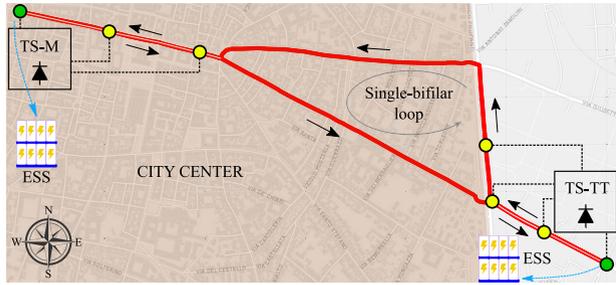
FIGURE 6. Topology of FS-MTT. Green circles indicate the position of supply feeders; yellow ones indicate the positions of reinforcement feeders. The ESSs are positioned in TS-M and TS-TT. Dashed lines represent the connection with the TSs. Arrows indicate the trolleybuses' travel direction.

The internal resistance of an SLB ($r_{\text{batt}}^{\text{SL}}$) is given by the one of a new battery ($r_{\text{batt}}^{\text{NB}}$) multiplied by a factor $\beta > 1$:

$$r_{\text{batt}}^{\text{SL}} = \beta \cdot r_{\text{batt}}^{\text{NB}}. \tag{26}$$

TABLE 1. Battery cell parameters.

Technology	V_{nom}	C_{nom}	MCR$_{\text{ds}}$	MCR$_{\text{ch}}$	r_{batt}	$\eta_{\text{batt}}^{\text{ds}}$	$\eta_{\text{batt}}^{\text{ch}}$
LTO$_1$ [28]	2.3 V	45 Ah	10 C	10 C	0.29 mΩ	94.3%	94.3%
LTO$_2$ [29]	2.2 V	70 Ah	7 C	7 C	0.43 mΩ	90.4%	90.4%
LTO$_3$ [30]	2.3 V	40 Ah	4 C	4 C	1.20 mΩ	91.6%	91.6%
LFP$_1$ [31]	3.2 V	15 Ah	5 C	3 C	4.00 mΩ	90.6%	94.3%
LFP$_2$ [32]	3.2 V	10 Ah	3 C	2 C	6.00 mΩ	94.4%	96.2%
LFP$_3$ [33]	3.2 V	228 Ah	1 C	1 C	0.22 mΩ	98.4%	98.4%
SLB	V_{nom}	λC_{nom}	γMCR$_{\text{ds}}$	γMCR$_{\text{ds}}$	βr_{batt}	$\eta_{\text{batt}}^{\text{ds}}$	$\eta_{\text{batt}}^{\text{ch}}$

Referring to (24), the efficiency of SLBs ($\eta_{\text{batt}}^{\text{SL}}$) can be given in function of NB parameters by:

$$\eta_{\text{batt}}^{\text{SL}} = 1 - \frac{\beta \cdot \gamma^2 \cdot r_{\text{batt}}^{\text{NB}} \cdot (I_{\text{batt}}^{\text{NB}})^2}{\gamma \cdot V_{\text{batt}}^{\text{NB}} \cdot I_{\text{batt}}^{\text{NB}}}. \tag{27}$$

Making the efficiency of SLBs equal to the efficiency of new ones ($\eta_{\text{batt}}^{\text{SL}} = \eta_{\text{batt}}^{\text{NB}}$), the outcome is:

$$\frac{r_{\text{batt}}^{\text{NB}} \cdot I_{\text{batt}}^{\text{NB}^2}}{V_{\text{batt}}^{\text{NB}} \cdot I_{\text{batt}}^{\text{NB}}} = \frac{\beta \cdot \gamma^2 \cdot r_{\text{batt}}^{\text{NB}} \cdot (I_{\text{batt}}^{\text{NB}})^2}{\gamma \cdot V_{\text{batt}}^{\text{NB}} \cdot I_{\text{batt}}^{\text{NB}}}. \tag{28}$$

Therefore, the γ factor is given as:

$$\gamma = \frac{1}{\beta}. \tag{29}$$

Note that Eq. 28 has not been reduced so as to keep a physical meaning to the parameters.

The battery cell parameters considered in the application under analysis are shown in Table 1: nominal voltage (V_{nom}), nominal capacity (C_{nom}), maximum C-rate during continuous operation for charge (MCR$_{\text{ch}}$) and discharge (MCR$_{\text{ds}}$), internal resistance, and efficiency during charge ($\eta_{\text{batt}}^{\text{ch}}$), and discharge ($\eta_{\text{batt}}^{\text{ds}}$). The efficiency values are calculated for each battery cell based on (24), considering their respective maximum continuous current during C&D processes. The last line shows the parameters considering a general SLB, where the internal resistance and the maximum current during C&D are respectively multiplied by the factors β and γ, as previously explained. The nominal capacity is multiplied
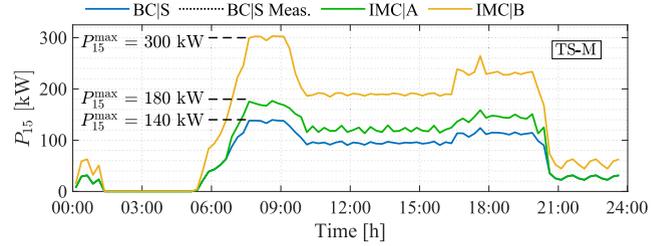
(a) Values of P_{15} in TS-M.
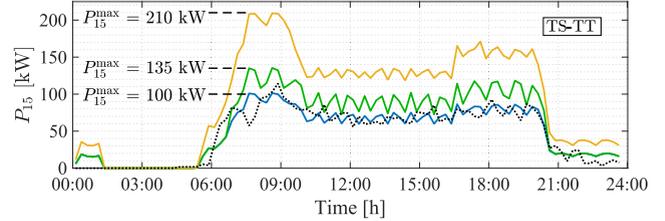
(b) Values of P_{15} in TS-TT.

FIGURE 7. Values of the 15-minute average power (P_{15}) and its maximum values (P_{15}^{max}) in TS-M and TS-TT for the scenarios under analysis.

by a factor λ representing the state of health (SOH) depreciation.

The selection of the battery cells for the analysis performed in this work was conducted through comprehensive research encompassing various datasheets from renowned brands of LTO and LFP battery manufacturers. The battery cell types were chosen based on MCR$_{\text{ch}}$, MCR$_{\text{ds}}$, and an efficiency of at least 90% for both C&D processes. As a result, three batteries were selected for each LTO and LFP type to cover a range of possible maximum values for the C&D rates. The first type was chosen for its capacity to withstand high rates, the second for medium rates, and the third for low rates.

IV. CASE STUDY: BOLOGNA'S TROLLEYBUS SYSTEM

The trolleybus system in the city of Bologna, Italy relies on an electrical infrastructure that includes multiple feeding sections (FSs). These FSs are powered by TSs typically located at either end. In this study, we focus on one of these FSs, called Marconi Trento-Trieste (FS-MTT), represented in Fig. 6. The FS-MTT is supplied by both TS-Marconi (TS-M) and TS Trento-Trieste (TS-TT). A 12-pulse diode rectifier generates a DC voltage with a rated value of 750 V at the output of the TS. To connect a TS to the OCL, supply feeders and auxiliary reinforcement feeders are used, represented by dashed lines in Fig. 6.

The initial route for trolleybuses operating within FS-MTT initiates near TS-M position, traverses along the southern side of the FS, and concludes in proximity to TS-TT, spanning a distance of 2200 m. Conversely, the return journey for trolleybuses takes the northern side and covers a distance of around 2500 m.

The city of Bologna has initiated the process of upgrading its trolleybus system by electrifying bus routes with vehicles equipped with IMC technology. Since the IMC trolleybuses are not yet operational in Bologna, this paper section focuses on examining hypothetical situations where IMC vehicles

coexist with traditional trolleybuses within the FS-MTT: The first scenario, referred to as IMC scenario A (IMC| A), assesses the catenary system with IMC trolleybuses running on line 15, while line 14 continues to be served by conventional trolleybuses; the second scenario (IMC| B) involves IMC vehicles exclusively on line 14. These theoretical scenarios are compared to the current setup, known as the base case scenario (BC| S), which involves only conventional trolleybuses in operation (refer to Table 2).

TABLE 2. Trolleybus lines in FS-MTT.

	Line 14	Line 15
BC|S	Conventional	Conventional
IMC|A	Conventional	IMC
IMC|B	IMC	Conventional

The evolution of power required by TS-M and TS-TT from the AC network, without the actuation of an ESS, in scenarios IMC| A and IMC| B in comparison to BC| S was determined by calculating averages over 15 min intervals, exhibited in Fig. 7. The notable increase in the 15 min average power supplied by the AC network (P_{15}) can be attributed not only to the extra power needed for charging the IMC vehicles' on-board battery but also to the difference from conventional trolleybuses, as IMC types do not inject braking energy to the grid. The power variation over time supplied by a TS to the trolleybus system in the BC| S scenario was confirmed through a one-day measurement conducted at TS-TT, exhibited in Fig. 7 as BC| S Meas. The data is from a November day, during the winter season in the northern hemisphere, when energy demand typically peaks due to the operation of heating systems within trolleybuses. Hence, the selected scenario for analysis mirrors a common instance of high energy demand. Details can be found in manuscript [34].

V. RESULT ANALYSIS CONSIDERING ESS ACTUATION

This section aims to assess the performance of an ESS composed of the battery cell types listed in Table 1 for the application under discussion. Best performance is achieved for the ESS that reduces P_{15}^{max} to the desired P_{ref} using minimal energy. The analysis is achieved through simulations encompassing three cases categorized by energy intensity of the ESS actuation: low, medium, and high. The goal is to discern a prevailing trend regarding the most suitable battery type for each of the three cases under consideration. The low energy intensity (LEI) case corresponds to the situation observed in TS-M under scenario IMC| A, while the medium energy intensity case (MEI) aligns with the situation found in TS-TT within the same scenario. The high energy intensity (HEI) case corresponds to both situations observed in TS-M and TS-TT in scenario IMC| B (Table 3).

TABLE 3. Energy intensity cases.

	TS-M	TS-TT
IMC|A	Low Energy Intensity (LEI)	Medium Energy Intensity (MEI)
IMC|B	High Energy Intensity (HEI)	High Energy Intensity (HEI)

(a) Values of P_{15}^{max} in TS-M.

(b) Values of P_{15}^{max} in TS-TT.
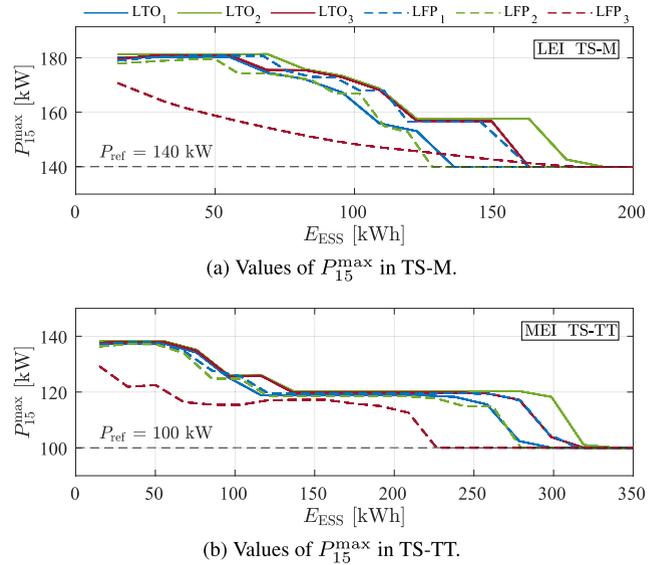
FIGURE 8. Maximum values of the 15-minute average power (P_{15}^{max}) in TS-M and TS-TT in scenario IMC| A using new LTO and LFP batteries.

(a) Values of P_{AC} and P_{15} in TS-M.
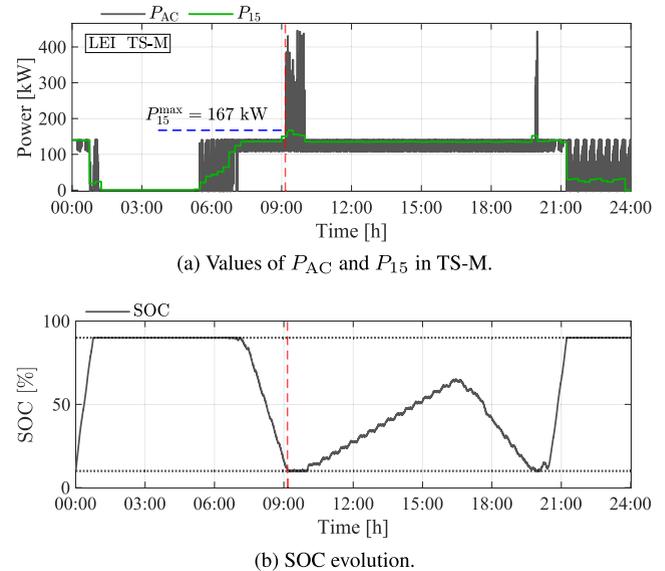
(b) SOC evolution.

FIGURE 9. P_{AC}, P_{15} and SOC evolution in scenario IMC| A, under actuation of a 100 kWh ESS made of LTO$_1$ cells. Blue dashed line indicates P_{15}^{max}; Red dashed line indicates the time when the SOC reaches 10%.

The simulations utilize P_{trll} data collected from TS-M and TS-TT and process it through the algorithm detailed in (Section III-B). The algorithm calculates the power handled by the ESS to keep P_{15} below the reference level (P_{ref}) at the same time that minimizes the ESS size. This is accomplished by charging and discharging activities defined by the threshold values P_{ch} and P_{ds}. The majority of the charging activities is designed to happen during periods of low power demand from the trolleybus network (e.g. at night between 21:00 and 06:00). The majority of discharging activities is designed to happen during the day between 06:00 up to 21:00 and have a high intensive activity during morning and afternoon peaks, from 06:00 and 10:30 and from 16:30 and 20:00 (Fig. 7). The battery state of charge (SOC)

is defined to stay in the range between $10\% \leq \text{SOC} \leq 90\%$. The converter is considered to operate in the power range (15) defined by $\alpha = 10\%$, and the operational efficiency is $\eta_{\text{conv}} = 96\%$ [26].

A. ESS PERFORMANCE EVALUATION IN SCENARIO IMC| A
In this scenario, the aim is to reduce the maximum value of the 15-minute average power (P_{15}^{max}) in TS-M from approximately 180 kW to $P_{\text{ref}} = 140$ kW (22.2%), and in TS-TT from 135 kW to $P_{\text{ref}} = 100$ kW (25.9%). Fig. 8 shows the relation between P_{15}^{max} and the required energy capacity of the ESS for the LTO and LFP battery types under consideration. The value of P_{15}^{max} decreases as the energy of the ESS increases. Small-energy ESSs discharge entirely early in the day and cannot act in the system significantly to lower P_{15}^{max} to the reference value after reaching the minimum SOC level. This is shown in Fig. 9 for a 100 kWh ESS made of LTO_1 cells acting in TS-M, as an example.

The reduction of P_{15} to the desired level in TS-M is classified as a LEI case because the amount of energy injected by the ESS takes place at major part during periods of morning and afternoon peaks. During off-peak hours, between 10:30 and 16:30, P_{15} remains below 140 kW in scenario IMC| A (Fig. 7 (a)). This indicates that ESS actuation to maintain P_{15} below P_{ref} is minor during these hours. Conversely, P_{15} reduction to the desired level in TS-TT is classified as a MEI case because the amount of energy injected by the ESS is also significant during off-peak hours because P_{15} in scenario IMC| B reaches the same level as 100 kW (Fig. 7 (b)).

Battery type comparison for TS-M, a LEI case, reveals that an ESS composed of LFP_3 or LTO_2 cells has the poorest performance, because the ESS has the largest battery size required to ensure P_{15} below or equal to P_{ref}. The former cell type operates with high efficiency but low C-rates; the latter tends to operate with the lowest efficiency values among the battery cells under consideration. Cell types with the highest performance are LFP_2 and LTO_1 because the required size of the ESS is the lowest. The mentioned cells present a good balance between efficiency and C-rate levels. Battery type performance for a LEI case can be ranked in (30), where E_{ESS} is the energy required by the ESS.

$$E_{\text{ESS}}^{\text{LFP}_2} < E_{\text{ESS}}^{\text{LTO}_1} < E_{\text{ESS}}^{\text{LFP}_1} \approx E_{\text{ESS}}^{\text{LTO}_3} < E_{\text{ESS}}^{\text{LFP}_3} \approx E_{\text{ESS}}^{\text{LTO}_2}. \quad (30)$$

The battery type comparison for TS-TT, a MEI case reveals that LTO_3 and LTO_2 have the poorest performance type, as shown in Fig. 8 (b). They also operate with the lowest efficiency rates during discharge among the analyzed cells. In contradiction to the LEI case, LFP_3 presents the best performance, indicating that, for MEI cases, high efficiency during operation is much more significant than high operational C-rates. The battery type performance for a MEI case can be ranked:

$$E_{\text{ESS}}^{\text{LFP}_3} < E_{\text{ESS}}^{\text{LFP}_2} < E_{\text{ESS}}^{\text{LTO}_1} < E_{\text{ESS}}^{\text{LFP}_1} \approx E_{\text{ESS}}^{\text{LTO}_3} < E_{\text{ESS}}^{\text{LTO}_2}. \quad (31)$$
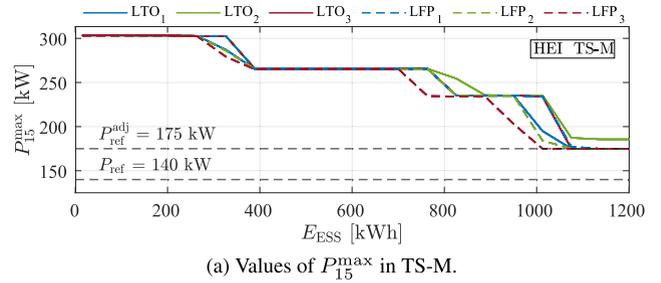
(a) Values of P_{15}^{max} in TS-M.
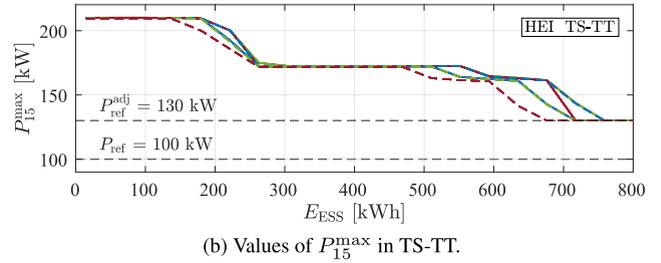
(b) Values of P_{15}^{max} in TS-TT.

FIGURE 10. Maximum values of the 15-minute average power (P_{15}^{max}) in TS-M and TS-TT in scenario IMC| B using new LTO and LFP batteries.

B. ESS PERFORMANCE EVALUATION IN SCENARIO IMC| B
The IMC| A scenario is a case where P_{15}^{max} value can be completely reduced to the one of BC| S so that the contract with the power utility would not change due to the insertion of IMC vehicles. However, this is not always possible with IMC| B because during HEI cases, there is a maximum value for reducing P_{15}^{max} when using ESSs. This is because there is a maximum amount of energy that the ESS can absorb from the AC network due to a limitation in the charging power and charging time. Charging power is constrained by an adjacent reference power, $P_{\text{ref}}^{\text{adj}}$, close to the desired P_{ref} value, while the charging duration is restricted by the nighttime when the trolleybus network's power demand is at its lowest (refer to Fig. 7). This nighttime period offers optimal conditions for the ESS to perform the majority of its charging. The maximum energy that the ESS can absorb from the AC network ($E_{\text{ESS}}^{\text{max}}$) is calculated by (32):

$$E_{\text{ESS}}^{\text{max}} = P_{\text{ref}}^{\text{ajd}} \cdot \Delta t_{\text{ch}}, \quad (32)$$

where Δt_{ch} is the charging time, defined for this analysis to be between 00:00 and 06:00, a total time of 6 hours.

Referring to TS-M, values of $E_{\text{ESS}}^{\text{max}}$ (column 2) for different $P_{\text{ref}}^{\text{adj}}$ (column 1) are exhibited in Table 4. For each of those values, one can verify if is possible to reduce P_{15}^{max} to the level of $P_{\text{ref}}^{\text{adj}}$ using the respective ESS size; results are displayed in column 3. Note that P_{15}^{max} is reduced to the level of $P_{\text{ref}}^{\text{adj}}$ for values from 250 kW to 175 kW. On the contrary, when $P_{\text{ref}}^{\text{adj}} = 170$ kW, P_{15}^{max} cannot be reduced to the desired level. Therefore, the theoretical limit for reducing P_{15}^{max}, carried out from 300 kW to 175 kW (41.7%) is found using an ESS of around 1050 kWh. Table 5 shows an analogous procedure carried out for TS-TT. One can observe that the maximum reduction of P_{15}^{max} is carried out from 210 kW to 130 kW (38%), which is reached using a 780 kWh ESS.

TABLE 4. Maximum storage energy (TS-M, IMC| B).

P_{ref}^{adj}	E_{ESS}^{max}	P_{15}^{max}
250 kW	1500 kWh	250 kW
200 kW	1200 kWh	200 kW
180 kW	1080 kWh	180 kW
175 kW	1050 kWh	175 kW
170 kW	1020 kWh	234 kW

TABLE 5. Maximum storage energy (TS-TT, IMC| B).

P_{ref}^{adj}	E_{ESS}^{max}	P_{15}^{max}
250 kW	1500 kWh	250 kW
200 kW	1200 kWh	200 kW
150 kW	900 kWh	150 kW
130 kW	780 kWh	130 kW
125 kW	750 kWh	141 kW

The relation between P_{15}^{max} and the required ESS energy composed by various battery cell types are illustrated in Fig. 10, for the two analyzed TSs. Similar to the MEI case, the best performance for HEI cases is observed for LFP_3 cells, while the poorest performance for LTO_2 ones. Consequently, the battery type performance for both substations can be ordered as follows:

$$E_{ESS}^{LFP_3} < E_{ESS}^{LFP_2} \approx E_{ESS}^{LTO_1} \approx E_{ESS}^{LFP_1} \approx E_{ESS}^{LTO_3} < E_{ESS}^{LTO_2}. \quad (33)$$

C. SECOND-LIFE BATTERIES PERFORMANCE EVALUATION

This section evaluates whether ESS composed of SLBs can be a viable option for the application under consideration. SLBs performance is evaluated in conservative scenarios, where simulations are carried out for β assuming values of 2 and 3 [35]. The battery SOH depreciation is fixed at 20%, therefore, $\lambda = 80\%$. It is worth noting here that although the number and depth of the charge and discharge cycles affect the battery degradation and, thereby, the system costs, this economic analysis is suggested for future work and is beyond the scope of this paper.

The impact of reducing P_{15}^{max} is shown in Fig. 11, comparing NBs and SLBs in scenarios IMC| A (LEI case) and IMC| B (MEI case), focusing on cells with the best performance in each instance. In the LEI case, utilizing SL LTO_1 demonstrates robust performance, unaffected by variations in internal resistance, as curves for $\beta = 2$ and $\beta = 3$ overlap. Conversely, the performance of SL LFP_2 cells is notably affected, displaying distinctive curves for $\beta = 2$ and $\beta = 3$, with the latter requiring a bigger ESS. This happens because of the C&D rate limitation, as with higher current limitations imposed in case of $\beta = 3$, the ESS is less capable of reducing the power peaks, which consequently affects the reduction of P_{15}^{max} to the desired P_{ref}. This is observable in Fig. 12 for a 160 kWh ESS made of LFP_2 cells, where the peaks power reduction is compromised due to the condition of $\beta = 3$ (Fig. 12 (b)) when compared to the case where $\beta = 2$ (Fig. 12 (a)). As a consequence, P_{15}^{max} is reduced to 141 kW, not enough to reach the desires P_{ref}. In MEI case, internal resistance variations have no impact
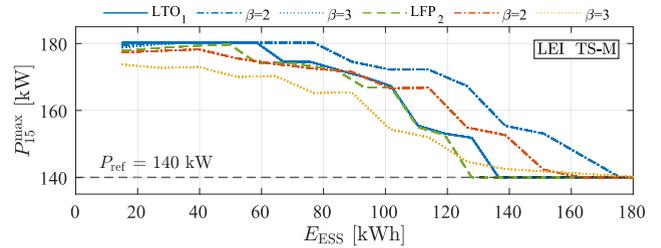
(a) Values of P_{15}^{max} in TS-M in scenario IMC|A.
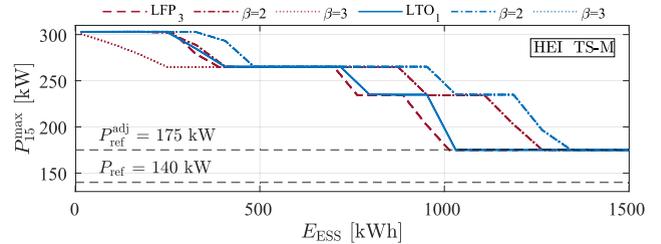
(b) Values of P_{15}^{max} in TS-M in scenario IMC|B

FIGURE 11. Comparing the performance of new and SL batteries. Internal resistance increase is denoted by factor $\beta = 2$ and $\beta = 3$; SOH depreciation is represented by factor $\lambda = 80\%$.
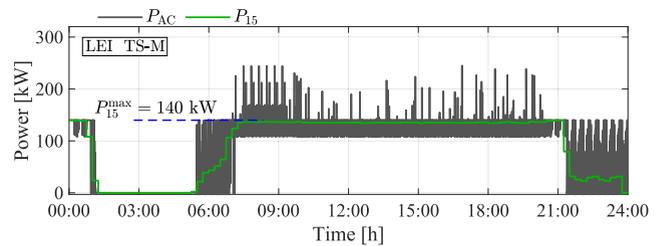
(a) Values of P_{AC} and P_{15} in TS-M for $\beta = 2$.
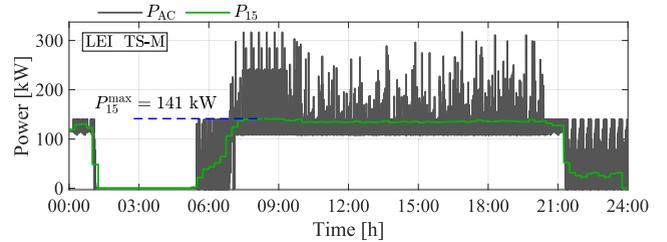
(b) Values of P_{AC} and P_{15} in TS-M for $\beta = 3$.

FIGURE 12. P_{AC} and P_{15} in TS-M in scenario IMC| A under actuation of a 160 kWh ESS made of LFP_2 cells. Blue dashed lines indicates P_{15}^{max}.

on performance, with superimposed curves for $\beta = 2$ and $\beta = 3$ using both LFP_3 and LTO_1 types. Notably, in both scenarios, a significant increase in the required ESS energy is observed when compared to new batteries (between 25% to 35%) to lower P_{15}^{max} to the reference value. The primary reason for that is attributed to the reduced nominal capacity resulting from SOH depreciation; the secondary reason is attributed to the C&D limitations imposed by γ values.

D. RESULTS ANALYSIS AND DISCUSSION

Batteries cells capable of handling high C-rates would generally be preferred to those limited to low C-rates (around 1C), for the majority of the applications. After completing the

analysis, this trend is confirmed for substations requiring low energy actuation from the ESS. However, an opposing trend emerged for substations requiring medium to high energy intensity ESS actuation. In these cases, batteries operating at low C-rates (1C) exhibited superior performance even compared to those capable of operating at 10C. The primary reason is that, with lower C-rates during operation, the ESS takes longer to be discharged up to the SOC limit (10%), and consequently, can supply to trolleygrid for a more extended period. The secondary reason concerns the higher efficiency during operation, leading to fewer losses in comparison to ESS able to discharge at high C-rates. Therefore, for the application under analysis, one can conclude that, as a general rule, ESSs composed of cells capable of operating at low C-rates tend to be preferred over those with high C-rates. However, in exceptional cases where TSs demand low energy actuation from the ESS, this study highlights the need for a trolleybus system to potentially incorporate two distinct types of ESS for each TS.

From the analysis of SLBs, there is an observed increase in the required energy amount ranging from 25% to 35%. In a scenario where transportation companies can get use of decommissioned batteries from their trolleybuses, SLB emerges as the most economically viable option, in the case that the price of SLB is lower by a factor of more than 35%, as compensation. This depends on a reduction in maximum current levels to ensure the operational efficiency of SLBs at the same level as the efficiency of new batteries. The only constraint is regarding the volume available inside TSs. Given that SLBs occupy a larger volume than NB, certain transportation companies may opt for new ones when faced with limited space. This consideration becomes particularly pertinent in the case of underground TSs situated in city centers. Concerning technology selection, both LTO and LFP are suitable ones. As a general trend, LFP_3 and LFP_2 are the most suitable for MEI and HEI cases, while LFP_2 and LTO_1 are the most suitable for LEI cases.

VI. CONCLUSION

This study performed a comparative analysis of different types of Lithium-ion battery cells, including second-life versions, to compose energy storage systems (ESSs) to be placed in traction substations (TSs), objecting to enable electrification projects in congested traction grid areas. The purpose of this work is to offer initial insights to transportation companies to aid them in their first decision-making process when selecting an appropriate battery technology for constructing stationary ESSs in TSs. In a case study of the city of Bologna, Italy, stationary ESSs were used to decrease the 15-minute average power demand (P_{15}), an important parameter defined in contractual agreements between the grid operator and transportation companies.

The work presents a tailored power management strategy designed to lower the maximum values of the 15-minute average power (P_{15}^{max}) to a user-defined threshold. This scheme guarantees the ESS charging under maximum power

conditions, resulting in a minimum required storage capacity. The proposed control scheme is adept at customizing the ESS size for the specific application under consideration and suggesting the most suitable technology. Results indicate that P_{15}^{max} can be reduced by up to 41.7% when a storage device actuates in TSs with high energy demand.

The best performance in reducing the P_{15} in a TS comes from ESSs capable of operating at high efficiency (around 94%). Meanwhile, high rates of charge and discharge (C&D) play a secondary role. Therefore, for this application, the general trend indicates that batteries capable of low C-rate operation are preferred over those with high C-rate capabilities, pointing toward less expensive cell types. In terms of technology, both Lithium Titanate Oxide (LTO) and Lithium Iron Phosphate (LFP) are viable options. The real selection will depend on comparing the number of cycles each cell can endure and the cost of each cycle per kilowatt-hour. In terms of cost, second-life batteries (SLBs) tend to be a competitive choice, but only if their maximum current setpoint is chosen so that it offers the same energy efficiency level as new batteries operating with their current setpoint chosen at the highest level. This means a reduction of SLBs maximum operation current as their internal resistance increases.

While this research offers insights into the energy capacity of storage systems relevant to the studied application, future endeavors should delve into the evaluation of the state of health degradation of individual cells due to C&D cycles and their impact on economic recommendations for each technology. A depreciation model of second-life batteries that also considers the intra-technology aspects of each battery cell should be used for this objective. This analysis can provide a broader comparison between the mentioned ESS technologies and strengthen the recommendations defined in this work.

REFERENCES

[1] S. Janssen, A. Fu, M. Cvetkovic, and P. Palensky, "Relocatable energy storage systems for congestion management," in *Proc. IEEE PES Innov. Smart Grid Technol. Eur. (ISGT-Europe)*, Oct. 2020, pp. 1166–1170.

[2] I. Diab, G. R. C. Mouli, and P. Bauer, "A review of the key technical and non-technical challenges for sustainable transportation electrification: A case for urban catenary buses," in *Proc. IEEE 20th Int. Power Electron. Motion Control Conf. (PEMC)*, Sep. 2022, pp. 439–448.

[3] I. Diab, B. Scheurwater, A. Saffirio, G. R. Chandra-Mouli, and P. Bauer, "Placement and sizing of solar PV and wind systems in trolleybus grids," *J. Cleaner Prod.*, vol. 352, Jun. 2022, Art. no. 131533.

[4] I. Diab, A. Saffirio, G. R. Chandra-Mouli, and P. Bauer, "A simple method for sizing and estimating the performance of PV systems in trolleybus grids," *J. Cleaner Prod.*, vol. 384, Jan. 2023, Art. no. 135623.

[5] K. van der Horst, I. Diab, G. R. Chandra Mouli, and P. Bauer, "Methods for increasing the potential of integration of EV chargers into the DC catenary of electric transport grids: A trolleygrid case study," *eTransportation*, vol. 18, Oct. 2023, Art. no. 100271.

[6] M. Bartłomiejczyk, L. Jarzebowicz, and R. Hrbác, "Application of traction supply system for charging electric cars," *Energies*, vol. 15, no. 4, p. 1448, Feb. 2022.

[7] S. Mohammed, D. Baumeister, M. Wazifehdust, P. Steinbusch, M. Zdrallek, S. Mour, P. Deskovic, T. Küll, and C. Troullier, "Impact assessment of integrating novel battery-trolleybuses, pv units and ev charging stations in a DC trolleybus network," in *Proc. E-Mobility Power Syst. Integr. Symp.*, 2018, pp. 1–6.

[8] R. F. P. Paternost, R. Mandrioli, R. Barbone, V. Cirimele, J. Loncarski, and M. Ricco, "Impact of a stationary energy storage system in a DC trolleybus network," in *Proc. IEEE Transp. Electrific. Conf. Expo (ITEC)*, Jun. 2022, pp. 1211–1216.

[9] R. F. P. Paternost, R. Mandrioli, M. Ricco, R. Barbone, G. Bonora, V. Cirimele, and G. Grandi, "Energy storage management in support of trolleybus traction power systems," in *Proc. Int. Symp. Power Electron., Electr. Drives, Autom. Motion (SPEEDAM)*, Jun. 2022, pp. 252–257.

[10] I. Diab, R. Eggermont, G. R. C. Mouli, and P. Bauer, "An adaptive battery charging method for the electrification of diesel or CNG buses as in-motion-charging trolleybuses," *IEEE Trans. Transport. Electrific.*, vol. 9, no. 3, pp. 4531–4540, Sep. 2023.

[11] Kiepe Electric. *IMC500/E-BUS With In-motion-charging (IMC)*. Accessed: May 31, 2023. [Online]. Available: https://kiepe.knorr-bremse.com/en/de/buses-and-e-mobilty/e-systems/imc500-e-bus-with-in-motion-charging-imc/

[12] M. Bartłomiejczyk, *Dynamic Charging of Electric Buses*. Sciendo, 2018. [Online]. Available: https://books.google.cz/books?id=ziX_vQEACAAJ and https://sciendo.com/book/9783110645088?tab=overview

[13] UITP. *In Motion Charging: Innovative Trolleybus*. Accessed: Dec. 7, 2021. [Online]. Available: https://cms.uitp.org/wp/wp-content/uploads/2021/01/Knowledge-Brief-Infrastructure-May-2019-FINAL.pdf

[14] N. A. El-Taweel, H. E. Z. Farag, and M. Mohamed, "Integrated utility-transit model for optimal configuration of battery electric bus systems," *IEEE Syst. J.*, vol. 14, no. 1, pp. 738–748, Mar. 2020.

[15] S. Hamacek, M. Bartlomiejczyk, R. Hrbáč, S. Mišák, and V. Stýskala, "Energy recovery effectiveness in trolleybus transport," *Electric Power Syst. Res.*, vol. 112, pp. 1–11, Jul. 2014.

[16] D. Iannuzzi, D. Lauria, and P. Tricoli, "Optimal design of stationary supercapacitors storage devices for light electrical transportation systems," *Optim. Eng.*, vol. 13, no. 4, pp. 689–704, Jul. 2011.

[17] A. González-Gil, R. Palacin, P. Batty, and J. P. Powell, "A systems approach to reduce urban rail energy consumption," *Energy Convers. Manage.*, vol. 80, pp. 509–524, Apr. 2014.

[18] S. Ahmadi, A. Dastfan, and M. Assili, "Energy saving in metro systems: Simultaneous optimization of stationary energy storage systems and speed profiles," *J. Rail Transp. Planning Manage.*, vol. 8, no. 1, pp. 78–90, Jun. 2018.

[19] A. Rufer, D. Hotellier, and P. Barrade, "A supercapacitor-based energy storage substation for voltage compensation in weak transportation networks," *IEEE Trans. Power Del.*, vol. 19, no. 2, pp. 629–636, Apr. 2004.

[20] D. Iannuzzi, F. Ciccarelli, and D. Lauria, "Stationary ultracapacitors storage device for improving energy saving and voltage profile of light transportation networks," *Transp. Res. C, Emerg. Technol.*, vol. 21, no. 1, pp. 321–337, Apr. 2012.

[21] K. Son, S. Noh, K. Kwon, J. Choi, and E.-K. Lee, "Line voltage regulation of urban transit systems using supercapacitors," in *Proc. IEEE Int. Power Electron. Motion Control Conf.*, May 2009, pp. 933–938.

[22] M. Jarnut, J. Kaniewski, and V. Protsiuk, "Energy storage system for peak-power reduction of traction substation," in *Proc. Innov. Mater. Technol. Electr. Eng. (i-MITEL)*, Apr. 2018, pp. 1–5.

[23] A. Okui, S. Hase, H. Shigeeda, T. Konishi, and T. Yoshi, "Application of energy storage system for railway transportation in Japan," in *Proc. Int. Power Electron. Conf.*, Jun. 2010, pp. 3117–3123.

[24] M. Khodaparastan, O. Dutta, and A. Mohamed, "Wayside energy storage system for peak demand reduction in electric rail systems," in *Proc. IEEE Ind. Appl. Soc. Annu. Meeting (IAS)*, Sep. 2018, pp. 1–5.

[25] A. Monticelli, *State Estimation in Electric Power Systems: A Generalized Approach*. Berlin, Germany: Springer, 2012.

[26] M. Forouzesh, Y. Shen, K. Yari, Y. P. Siwakoti, and F. Blaabjerg, "High-efficiency high step-up DC–DC converter with dual coupled inductors for grid-connected photovoltaic systems," *IEEE Trans. Power Electron.*, vol. 33, no. 7, pp. 5967–5982, Jul. 2018.

[27] A.-I. Stan, M. Swierczynski, D.-I. Stroe, R. Teodorescu, S. J. Andreasen, and K. Moth, "A comparative study of lithium ion to lead acid batteries for use in ups applications," in *Proc. IEEE Int. Telecommun. Energy Conf.*, Sep. 2014, pp. 1–8.

[28] GWL Group. *LTO Yinlong 2.3V 45Ah Battery*. Accessed: Sep. 13, 2023. [Online]. Available: https://files.gwl.eu/inc/_doc/attach/StoItem/7777/LTO-45AH-CY_datasheet.pdf

[29] Altairnano. *70 AMP Hour Cell*. Accessed: Sep. 13, 2023. [Online]. Available: https://altairnano.com/products/70-amp-hour-cell/

[30] Selian Energy. *LTO Yinlong 2.3V 40Ah Battery*. Accessed: Sep. 13, 2023. [Online]. Available: https://selianenergy.com/

[31] AA Portable Power Corp. *LFP Battery Specification Model: LFP-40152S 3.2V 15Ah*. Accessed: Sep. 13, 2023. [Online]. Available: www.batteryspace.com/prod-specs/7493.pdf

[32] Elerix. *Technical Specification Elerix EX-L10: High Energy Density Storage LFP Cell*. Accessed: Sep. 13, 2023. [Online]. Available: https://elerix.com/wp-content/uploads/2023/05/baterie_EX-L10_2.pdf

[33] EV lithium. *CATL 3.2V 228Ah LiFePO4 Prismatic Battery Cell*. Accessed: Sep. 13, 2023. [Online]. Available: www.evlithium.com/catl-battery-cell/catl-228ah-lifepo4-battery.html

[34] R. F. Paternost, R. Mandrioli, R. Barbone, M. Ricco, V. Cirimele, and G. Grandi, "Catenary-powered electric traction network modeling: A data-driven analysis for trolleybus system simulation," *World Electric Vehicle J.*, vol. 13, no. 9, p. 169, Sep. 2022.

[35] A.-I. Stroe, D.-L. Stroe, V. Knap, M. Swierczynski, and R. Teodorescu, "Accelerated lifetime testing of high power lithium titanate oxide batteries," in *Proc. IEEE Energy Convers. Congr. Expo. (ECCE)*, Sep. 2018, pp. 3857–3863.

RUDOLF F. P. PATERNOST received the bachelor's degree in electrical engineering from the University of São Paulo, Brazil, in 2017, the master's degree in electrical engineering from the University of Campinas, Brazil, in 2019, and the Ph.D. degree in automotive engineering for intelligent mobility from the Department of Electrical, Electronic, and Information Engineering, University of Bologna, Italy, in 2024. During this period, he was also involved as a Teaching Assistant for engineering courses. In 2023, he was a Visiting Ph.D. Student with the Electrical Engineering Faculty, Delft University of Technology (TU Delft). His activities center on proposing solutions to modernize the electrical infrastructure of catenary-powered transportation systems, preparing them to integrate emerging technologies, such as in-motion-charging vehicles, energy storage systems, and electric vehicles, which are expected to become more prevalent in the future.

IBRAHIM DIAB (Member, IEEE) received the bachelor's degree in mechanical engineering from American University of Beirut, in 2012, and the Ph.D. degree from the DCE&S Group, Electrical Engineering Faculty, Delft University of Technology (TU Delft), on transforming the trolleybus grid into an active, sustainable, and multi-functional electrical infrastructure. In 2015, he received the TU Delft "Delft Research Initiative-Energy" Full Scholarship and joined the Sustainable Energy Technologies (SET) master's program of the Electrical Engineering Faculty (2017, honors).

After graduating, he started with the DCE&S Group as a full-time Teaching Assistant on courses, such as ac and dc microgrids, electrical power conversion, and the system integration project. Then, he worked as a co-creator and the manager for the Professional Certificates online courses of the ESE Department on intelligent electrical power grids, and electrical power conversion. From September 2022 to March 2024, he was a Postdoctoral Research Fellow jointly at the AMS Institute, Amsterdam, and the DCE&S Group, TU Delft, on integrating electric bus chargers in the metro grid of Amsterdam. Since January 2024, he has been a Private Consultant working on a number of Dutch and European projects, such as multi-functional trolleybus grids, EV charging infrastructures, circularity in transport grids, and dc energy hubs.

GAUTHAM RAM CHANDRA MOULI (Member, IEEE) received the bachelor's degree from the National Institute of Technology, Trichy, India, in 2011, the master's degrees in electrical engineering from Delft University of Technology, The Netherlands, in 2013, and the Ph.D. degree for the development of a solar-powered V2G electric vehicle charger compatible with CHAdeMO, CCS/COMBO, and designed smart charging algorithms (with PRE, ABB, and UT Austin) from Delft University in 2018. From 2017 to 2019, he was a Postdoctoral Researcher at TU Delft pursuing his research on power converters for EV charging, smart charging of EVs, and trolley busses. He is a coordinator and a Lecturer for Massive Open Online Course (MOOC) on Electric cars on edX.org with 200 000 learners from 175 countries. He is a tenured Assistant Professor in the dc systems, energy conversion and storage group with the Department of Electrical Sustainable Energy, Delft University of Technology. His current research interests include electric vehicles and charging, PV systems, power electronics, and intelligent control. He was awarded the Best Paper Prize Award from IEEE Transactions on Industrial Informatics in 2018, the Best Poster Prize at Erasmus Energy Forum 2016, The Netherlands, and the Best Paper Prize at the IEEE INDICON Conference 2009, India. It was awarded the 'Most significant innovation in electric vehicles' award from IDtechEx in 2018, and the 'Best Tech Idea of 2018' by KIJK. He is involved in many projects with industrial and academic partners at national and EU levels concerning electric mobility and energy storage such as OSCD, Trolley 2.0, Flexinet, TULIPS, FLOW, Drive2X, and NEON. He is the Vice-Chair of the IEEE Industrial Electronic Society Benelux chapter.

PAVOL BAUER (Senior Member, IEEE) received the master's degree in electrical engineering from the Technical University of Kosice, Koisce, Slovakia, in 1985, and the Ph.D. degree from Delft University of Technology, Delft, The Netherlands, in 1995. He is currently a Full Professor with the Department of Electrical Sustainable Energy, Delft University of Technology; the Head of the DC Systems, Energy Conversion and Storage Group; a Professor with Brno University of Technology, Brno, Czechia; and the Honorary Professor with Politehnica University Timisoara, Timisoara, Romania. From 2002 to 2003, he was with KEMA (DNV GL, Arnhem) on different projects related to power electronics applications in power systems. He has authored and co-authored more than 120 journals and 500 conference papers in his field with H-factor Google scholar 40, and Web of Science 26, he is the author or co-author of eight books, holds seven international patents, and organized several tutorials at international conferences. He has worked on many projects for industry concerning wind and wave energy, power electronic applications for power systems such as Smarttrafo, HVdc systems, projects for smart cities such as PV charging of electric vehicles, PV and storage integration, contactless charging, and participated in several Leonardo da Vinci, H2020 and Electric Mobility Europe EU projects as a Project Partner (ELINA, INETELE, E-Pragmatic, Micact, Trolley 2.0, OSCD, P2P, Progressus) and a Coordinator (PEMCWebLab.com-Edipe, SustEner, Eranet DCMICRO). His main research focuses on power electronics for charging of electric vehicles and dc grids. He is the Former Chair of the Benelux IEEE Joint Industry Applications Society, Power Electronics and Power Engineering Society chapter, the Chairman of the Power Electronics and Motion Control council, Member of the Executive Committee of European Power Electronics Association and the International Steering Committee at numerous conferences.

MATTIA RICCO (Senior Member, IEEE) received the master's degree (cum laude) in electronic engineering from the University of Salerno, Fisciano, Italy, in 2011, and the double Ph.D. degrees in electrical and electronic engineering and information engineering from the University of Cergy-Pontoise, Cergy-Pontoise, France, and the University of Salerno, in 2015.

From 2015 to 2018, he was a Postdoctoral Research Fellow with the Department of Energy Technology, Aalborg University, Aalborg, Denmark. From 2018 to 2021, he was a Senior Assistant Professor (tenure track) and has been an Associate Professor with the Department of Electrical, Electronic, and Information Engineering, University of Bologna, Bologna, Italy, since 2021. His research interests include modular multilevel converters, battery management systems, electric vehicle chargers, field-programmable gate array-based controllers, identification algorithms for power electronics, and photovoltaic systems.

GABRIELE GRANDI (Senior Member, IEEE) received the M.Sc. (cum laude) and Ph.D. degrees in electrical engineering from the University of Bologna, Bologna, Italy, in 1990 and 1994, respectively.

He has been with the Department of Electrical, Electronic, and Information Engineering, University of Bologna, as a Research Associate, since 1995; an Associate Professor, since 2005, and a Full Professor of electrical engineering, since 2016. He is currently the Director of bachelor's and master's programs in electrical engineering with the University of Bologna. He is also the Founder and the Leader of the Research Laboratory "SolarTronic-Lab," University of Bologna, dealing with power electronic circuits, multiphase and multilevel converters, photovoltaic, electric vehicle chargers, and circuit modeling. He has authored or co-authored more than 180 papers published in conference proceedings and international journals, mainly with IEEE. He is an Editor of *IET Power Electronics* "Rapid Communications," and an Associate Editor of IEEE Transactions on Industrial Electronics and IEEE Transactions on Power Electronics.

● ● ●